



## Short communication

# Metal current collector-free freestanding silicon–carbon 1D nanocomposites for ultralight anodes in lithium ion batteries

Jang Wook Choi, Liangbing Hu, Lifeng Cui, James R. McDonough, Yi Cui\*

Department of Materials Science and Engineering, Stanford University, 476 Lomita Mall, Stanford, CA 94305, USA

## ARTICLE INFO

## Article history:

Received 12 May 2010

Received in revised form 24 June 2010

Accepted 27 June 2010

Available online 13 July 2010

## Keywords:

Current collector

Li-ion battery

Nanowire

Nanofiber

## ABSTRACT

Although current collectors take up more weight than active materials in most lithium ion battery cells, so far research has been focused mainly on improving gravimetric capacities of active materials. To address this issue of improving gravimetric capacities based on overall cell components, we develop freestanding nanocomposites made of carbon nanofibers (CNFs) and silicon nanowires (SiNWs) as metal current collector-free anode platforms. Intrinsically large capacities of SiNWs as active materials in conjunction with the light nature of freestanding CNF films allow the nanocomposites to achieve 3–5 times improved gravimetric capacities compared to what have been reported in the literature. Moreover, three-dimensional porous structures in the CNF films facilitate increased mass loadings of SiNWs when compared to flat substrates and result in good cycle lives over 40 cycles. This type of nanocomposite cell suggests that 3D porous platforms consisting of light nanomaterials can provide for higher gravimetric and areal capacities when compared to conventional battery cells based on flat, heavy metal substrates.

© 2010 Elsevier B.V. All rights reserved.

## 1. Introduction

Recently, significant efforts have been made to develop energy storage devices with large capacities to keep pace with their ever-growing demand in various applications such as portable electronic devices and electrical vehicles. Lithium (Li) ion rechargeable batteries have been pivotal in those efforts due to their superior gravimetric and volumetric capacities compared to those of other batteries [1]. Typical battery cells consist of several components [2] including active electrodes, current collectors, electrolytes, and separators. Therefore, developing light materials for each component could contribute as much or more to improving gravimetric capacities as simply finding higher capacity active materials. In particular, development of light current collectors can substantially improve capacities because current collectors take up more weight than active materials in most Li-ion batteries. Recently, we found that office paper used in our everyday lives for documentation can be used as light and robust current collectors for Li-ion batteries when integrated with carbon nanotubes [3]. In our estimation, paper can result in a 20–30% weight reduction compared to typical metal current collectors when the same active materials are used. This weight reduction is from the calculation based on all cell components including active materials, carbon nanotubes and paper. By integration with carbon nanotubes, insulating paper can become conductive and the sheet resistance of the conductive

paper reaches down to  $\sim 10 \Omega \text{sq}^{-1}$ . We also provided a calculation showing that modified cell designs compatible with 18,650 cells can lead to the total electrode resistances as low as  $25 \text{m}\Omega$  based on both anode and cathode sides. This value is lower than the internal resistance of practical Li-ion batteries thus confirming that the conductive paper can be used without conductivity issue. On the other hand, silicon has been one of the most promising anode active materials due to its extraordinary capacity. Its theoretical capacity, around  $4000 \text{mAh g}^{-1}$ , is more than 10 times larger than currently existing graphite anodes in commercial Li-ion batteries. Despite the superior capacity, its large volume change ( $\sim 300\%$  upon full lithiation) causes pulverization of the electrodes and thus severe capacity fading [4]. As a solution to minimize this pulverization issue, several approaches including using various nanostructures [5,6] and nanocomposites [7,8] have been tested. Recently, we have investigated various one-dimensional (1D) silicon nanostructures as anode materials [9–11]. The facile strain relaxation enabled by unique 1D nanostructures results in a high capacity ( $>3000 \text{mAh g}^{-1}$ ) and a good cycle life ( $>50$  cycles). Inspired by the substantial weight reduction associated with light current collectors as well as the advantages of 1D nanostructures as active materials, here we develop a metal current collector-free nanocomposite of silicon and carbon 1D nanomaterials in order to improve the gravimetric device capacities further (Fig. 1). Carbon nanofibers (CNFs) were used to form a film functioning as a light current collector. Silicon nanowires (SiNWs) grown on the surfaces of and inside the CNF film function as high capacity active materials. In order to address the considerable advantage in the gravimetric energy density (or capacity per gram) related

\* Corresponding author. Tel.: +1 650 723 4613; fax: +1 650 725 4034.  
E-mail address: [yicui@stanford.edu](mailto:yicui@stanford.edu) (Y. Cui).

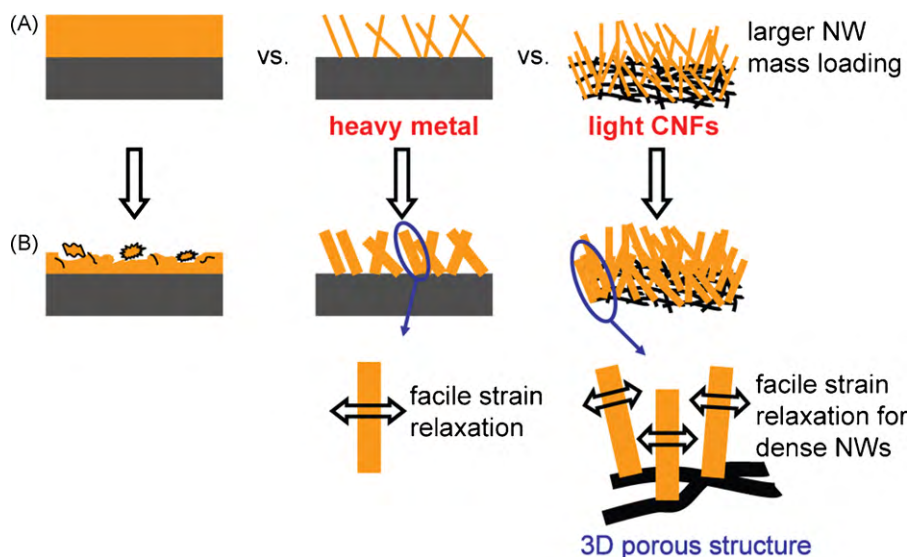


**Fig. 1.** (A) A schematic comparison of a silicon layer on a metal current collector to SiNWs on a flat metal current collector to SiNWs on a light CNF film before cycling. The 3D porous structure of the CNF film facilitates a larger number of SiNWs compared to SiNWs on the flat substrate. (B) A schematic illustration of those three cases after cycling. The silicon layer becomes easily pulverized due to the volume expansion. A unique combination of the 1D structures of SiNWs and the 3D porous structure of the CNF film allows facile strain relaxation for dense NWs during cycling.

to the light nanomaterial based current collectors, we use the combined mass of the active material and current collector as a primary metric and use this metric for a fair comparison with existing other anode platforms in a consistent manner. Assuming that these freestanding platforms are used in commercial 18,650 cells whose typical areal capacities are  $\sim 4 \text{ mAh cm}^{-2}$ ,  $\sim 23\%$  mass reduction is expected on the anode side (Table 2).

## 2. Experimental

### 2.1. The preparation of CNF–SiNW nanocomposites

The freestanding nanocomposite was first prepared by making a carbon nanofiber (CNF) ink. An aqueous mixture of CNFs, polyvinyl alcohol (PVA), and sodium dodecylbenzene sulfonate (SDBS) (1–2, 0.5–1, 0.5–1% by weight, respectively, all chemicals purchased from Sigma–Aldrich) was sonicated until the ink became completely homogenous. PVA was used to improve the mechanical stability of the freestanding CNF film and SDBS was used as a surfactant. Next, the ink was suctioned into alumina membranes (Whatman, 200 nm in pore width) using vacuum filtration. Once CNF solution was transferred, the films were washed thoroughly with isopropanol using vacuum filtration to remove residual surfactants and thus improve film conductivities. Finally, the alumina membranes were removed by dipping them in 1.25 M sodium hydroxide solution. These steps typically yielded CNF films that were  $\sim 0.8 \text{ mg cm}^{-2}$  and  $\sim 20 \text{ }\mu\text{m}$  thick with sheet resistances of  $20\text{--}80 \text{ }\Omega \text{ sq}^{-1}$ . Also, the film is mechanically stable such that the film can be held with tweezers as a freestanding platform. Other types of membranes could be used instead of alumina membranes as long as they can be removed without damaging the CNF layers. Next, a 20 nm layer of gold was thermally deposited for use as a catalyst in the subsequent SiNW vapor–liquid–solid (VLS) growth. Detailed procedures for the SiNW growth were described previously [12]. After the growth, the originally black CNF film changed to a brown CNF–SiNW nanocomposite (Fig. 2A). These nanocomposites enable increased silicon mass loadings per area compared to planar substrate geometries (Fig. 1). After identical growth processes, silicon mass increases for CNF films and flat stainless steel substrates are 1.2–2.8 and 0.3–0.7  $\text{mg cm}^{-2}$ , respectively. Again, this significant improvement

of active materials mass per area is attributed to the porous structure of three-dimensional CNFs networks. Similar improved mass loadings have been demonstrated using 3D porous metal substrates such as nickel foam [13]. However, metal substrates are heavier and are therefore not beneficial for overall device gravimetric capacities.

### 2.2. The electrochemical testing

The CNF–SiNW nanocomposites were tested as half cells by preparing pouch cells (Fig. 3A). Lithium metal foil (Alfa Aesar) was used as the counter electrode in each cell. A 1 M solution of  $\text{LiPF}_6$  in ethylene carbonate/diethyl carbonate (EC/DEC, 1:1 v/v, Ferro Corporation) was used as the electrolyte with separators from Asahi Kasei. Cells were assembled in an argon-filled glovebox.

## 3. Results and discussion

Fig. 2B and C shows scanning electron microscopy (SEM) images for a bare CNF film and a CNF–SiNW nanocomposite after the growth process. SiNWs are mainly on the surface where gold layers were deposited (Fig. 2C). But, some SiNWs penetrate into CNF films because gold catalyst layers are broken into nanoparticles, and the nanoparticles diffuse into the CNF layers during the VLS growth. A transmission electron microscope (TEM) image for the sample scratched off the surface of the nanocomposite is presented in Fig. 2D. A selected area electron diffraction (SAED) pattern that was obtained for the middle of a SiNW confirms that SiNWs generated from the VLS growth are single crystalline (Fig. 2D). One noteworthy point is the inherently firm binding of SiNWs onto the CNF films as a result of the VLS process (dotted circles in Fig. 2D). A high resolution (HR) TEM image clearly visualizes the firm binding between CNFs and SiNWs (Fig. 2E). This unique, advantageous feature allows SiNWs to remain well-bound during cycling and thus achieve a good cycle life. Also, the silicon to carbon mass ratio can be controlled by growth time, and for most samples the ratio is 2–5. Energy-dispersive X-ray spectroscopy (EDS) data (Fig. 2F) also confirm a greater amount of silicon relative to other elements.

The cell structure is illustrated in Fig. 3A. In Fig. 3B, potential profiles measured at different numbers of cycles are presented

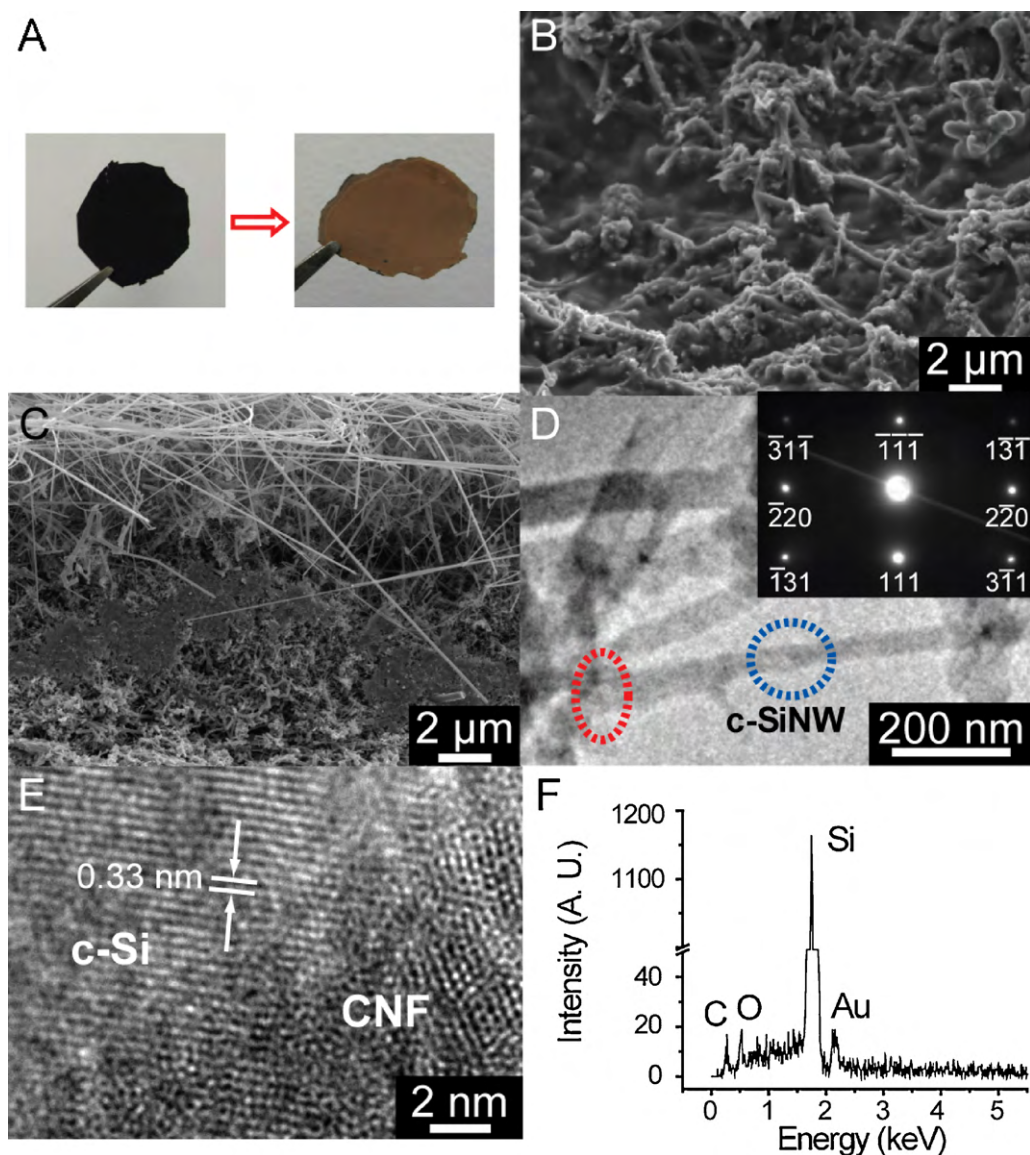


**Fig. 2.** (A) Photographs of a freestanding CNF film before and after SiNW growth. SEM images of (B) a bare CNF film and (C) a cross-section of a CNF-SiNW nanocomposite. (D) A TEM image showing SiNWs are well-bound onto CNFs. A SAED pattern (inset) obtained over the blue dotted circle confirms the single crystalline nature of SiNWs. (E) A HRTEM image for the red dotted circle in (D) shows the interface between a SiNW and a CNF and verifies the firm binding between those 1D nanomaterials. (F) EDS data for the CNF-SiNW nanocomposite. (For interpretation of the references to color in this figure legend, the reader is referred to the web version of the article.)

for a cell with a  $3.6 \text{ mg cm}^{-2}$  mass loading (including both carbon and silicon) operated at a  $C/10$  charging/discharging rate. The charge/discharge rates were calculated based on the theoretical capacities of silicon ( $4200 \text{ mAh g}^{-1}$ ) and CNF ( $300 \text{ mAh g}^{-1}$ ) and the mass ratio of 4 (Si:C):  $1C = 3.42 \text{ A g}^{-1}$ . A plateau at  $0.12 \text{ V}$  in the charging process of the first cycle indicates crystalline silicon is the dominant active material [11,14]. Although some amorphous silicon shell layers were deposited onto CNFs during the VLS growth, their amounts were relatively smaller compared to those of crystalline silicon. Control samples without gold catalyst layers gain less than  $1/10$  mass increase after the same growth process. Also, the hysteresis between charge/discharge curves (Fig. 3B) is  $\sim 0.39 \text{ V}$  when measured between the middle points of charge/discharge curves. This value is the same as that of SiNWs grown on flat substrates [11], which indicates the higher sheet resistances of the CNF films compared to metal current collectors are not the limiting factor for battery operations at least for these several  $\text{cm}^2$  scale and the contact with metal foils that are used for electrical reach-out for measurement at the edge of the nanocomposite (Fig. 3A) is not

also limiting. In all the battery data described in Fig. 3, charging cut-off potentials were set to  $10 \text{ mV vs. Li/Li}^+$  so that the crystalline silicon becomes amorphous during the first charge. This transition is confirmed by potential profiles which have steeper slopes in the second and subsequent cycles.

Fig. 3C shows capacity retention data for samples with different mass loadings. These capacity retention data imply several important points. First, the nanocomposite devices show comparable capacity retentions to those of similar devices on flat substrates [10,11] even though the masses of active materials per area of the substrates are significantly higher. This comparable cycle life can be attributed to the porous 3D structure of CNF networks. SiNWs grown within the 3D structures can utilize the ample space between NWs for facile strain relaxation during cycling. Second, cycle life is correlated with the mass of active materials. While a sample with  $2.0 \text{ mg cm}^{-2}$  loses  $\sim 12\%$  of the initial capacitance after 40 cycles, the one with  $3.6 \text{ mg cm}^{-2}$  exhibits a more rapid capacity decay even though the one with  $2.0 \text{ mg cm}^{-2}$  was charged and discharged at a higher rate ( $C/2$  vs.  $C/10$ ). This mass dependence

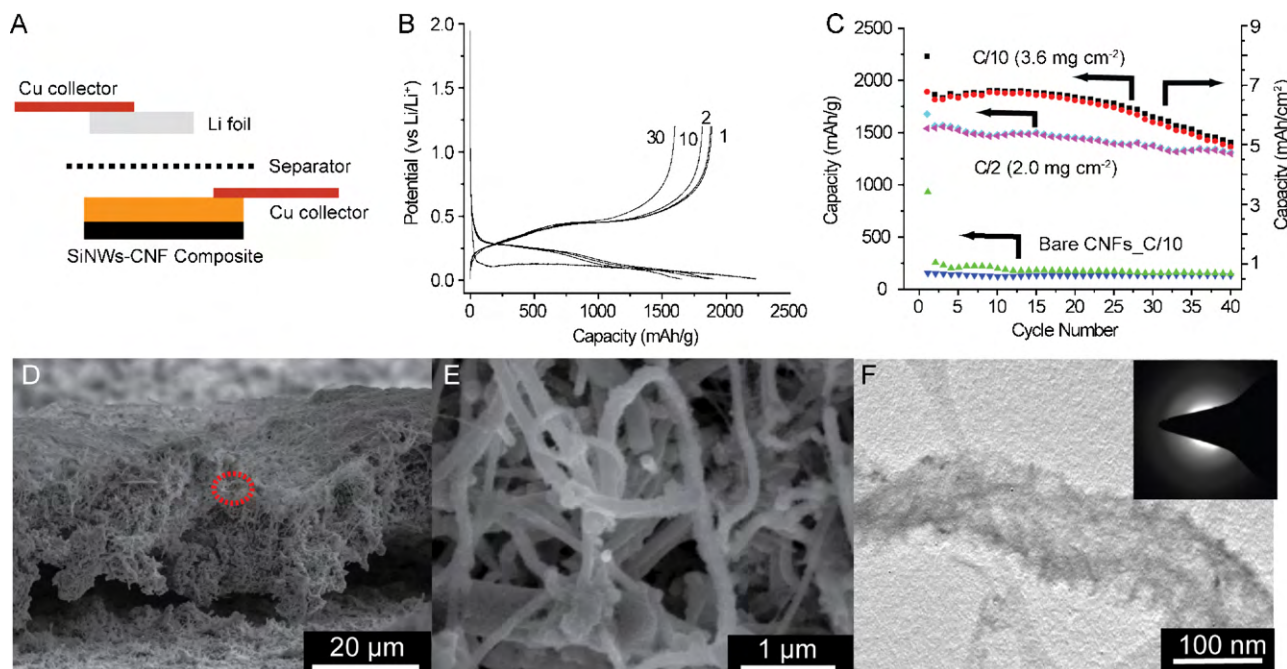


**Fig. 3.** (A) A schematic illustration of a half-cell used for testing CNF-SiNW nanocomposites as anodes. (B) Charging and discharging profiles from the half-cell tests measured at different numbers of cycles. The cycle numbers are denoted next to each discharging potential plot. (C) Capacity retention data for CNF-SiNW nanocomposites with different mass loadings and charging/discharging rates as well as those for a control sample with bare CNFs. Capacities are based on the combined mass of both CNFs and SiNWs. The symbols in black, cyan, and green are for charging and the symbols in red, purple, and blue are for discharging. (D) An SEM image of a CNF-SiNW nanocomposite after 5 cycles. (E) A higher magnification SEM image for the region marked with the red dotted circle in (D). (F) A TEM image of a SiNW after 5 cycles with its SAED pattern (inset) indicating the rough surface as well as the amorphous structure. (For interpretation of the references to color in this figure legend, the reader is referred to the web version of the article.)

suggests that the strain exerted on the active materials cannot be relaxed efficiently above a certain mass loading. With a large SiNW mass loading, free space between SiNWs might not be large enough for efficient strain relaxation. Third, during cycling the areal capacity remains above  $5 \text{ mAh cm}^{-2}$  for the sample with a  $3.6 \text{ mg cm}^{-2}$  mass loading and therefore is even larger than most of commercial devices. Coulombic efficiencies of the sample with a  $2.0 \text{ mg cm}^{-2}$  mass are 91.8% in the first cycle and larger than 99% in all subsequent cycles. The other sample with a  $3.6 \text{ mg cm}^{-2}$  mass exhibits lower Coulombic efficiency, perhaps due to the larger mass loading, such that Coulombic efficiencies are 84.7% in the first cycle and 96.5–99.2% in the subsequent cycles. The Coulombic efficiency data are presented in [Supplementary Materials](#). Finally, control experiments with bare CNF films show a discharging (delithiation) capacity of  $150 \text{ mAh g}^{-1}$  in the first cycle. However, this value continuously decreases to  $125 \text{ mAh g}^{-1}$  during 50 cycles. This decrease might be due to Faradaic reaction of CNFs with  $\text{Li}^+$  during cycling. However, PVA that is originally included in the ink is likely to be helpful in mechanically holding the film structure throughout cycles. A relatively large but irreversible capacity in the first charging (lithiation) process might be related to solid-electrolyte interface (SEI) formation on the CNF surface as the plateau location ( $\sim 0.8 \text{ V}$ ) is consistent with the potential where the standard electrolyte used in this study is decomposed. It is noteworthy that remarkably improved Coulombic efficiencies of the CNF-SiNWs in the first cycle compared to the bare CNFs indicate that silicon layers deposited on the surfaces of CNFs play a critical role for the reversible cycling.

SEM images in [Fig. 3D](#) and [E](#) show cross-sections of the nanocomposite and SiNW morphologies after 5 cycles. SiNWs become bent due to unbalanced NW volume expansions during the cycling, which is consistent with our previous observations [\[11\]](#) based on flat substrates. Also, the surfaces of SiNWs in the HRTEM image ([Fig. 3F](#)) appear rougher than those of pristine NWs.

Previously, we learned that this rougher surface originates from slow atomic diffusion of silicon during cycling. In fact, the cycling not only makes the surfaces of SiNWs rough, but also generates nanopores inside SiNWs [\[12\]](#). Due to the slow atomic diffusion, the NW crystal structure changes from single crystalline to amorphous during the cycling, as shown in a selected area electron diffraction pattern in [Fig. 3F](#). Similar overall nanocomposite thicknesses ( $\sim 20 \mu\text{m}$ ) before and after cycling also confirm the robust mechanical properties of the nanocomposite.

The gravimetric capacities and energy densities of these metal current collector-free nanocomposite cells stand out impressively when compared to those of other types of cells built on heavy metal substrates. These improvements stem from both the extremely high capacity of Si and thus the lower mass loading of active anode materials required to achieve the same areal performance as commercial devices and also from the elimination of heavy metallic current collectors on the anode side. In most gravimetric data reported in the literature, the mass loading of active materials is less than  $1 \text{ mg cm}^{-2}$  which means that if metal current collector masses ( $5\text{--}14 \text{ mg cm}^{-2}$  for Cu) are also included in the masses used to calculate the gravimetric data, the results become much worse than their reported values. In order to see the significance of using CNF films as light current collectors, we found capacity data for anode materials in a half-cell configuration (SiNWs [\[11\]](#), metal oxide [\[15\]](#), tin [\[16\]](#), tin-copper alloy [\[17\]](#), mesocarbon composite [\[18\]](#), commercial graphite) with active material mass loadings larger than  $5 \text{ mg cm}^{-2}$  in the literature. The data are summarized in [Table 1](#). In the case of the metal substrate-based cells, even if we assume that the lightest metal current collectors ( $\sim 5 \text{ mg cm}^{-2}$ ) can be used, the specific capacities of most cells decrease to 1/6 to 2/3 of those based on the active materials only. In contrast, the capacity of our nanocomposites remains the highest value at  $1500 \text{ mAh g}^{-1}$ . The absence of metal current collectors also improves specific energy densities remarkably in a full cell configuration. When the masses of other

**Table 1**  
Gravimetric capacities of various anodes based on both active materials and current collectors (half-cell configuration).

	Active material mass ( $\text{mg cm}^{-2}$ )	Capacities (active material only) ( $\text{mAh g}^{-1}$ )	Capacities (active material + current collector) ( $\text{mAh g}^{-1}$ ) <sup>b</sup>	Reference
Freestanding CNT-SiNW	3	1500	1500	–
SiNWs on Cu	1	3000	500	[11]
Metal oxide on Cu	10	900	600	[15]
Sn on Cu	7.2	600	354	[16]
Cu-Sn alloy	6	350	191	[17]
Mesocarbon composite	67.5	340	317	[18]
Commercial graphite on Cu	13.52 <sup>a</sup>	372	271	–

<sup>a</sup> This value is for a cell with an areal capacity of  $4 \text{ mAh cm}^{-2}$ .

<sup>b</sup> For the Cu current collector, the lightest mass of  $5 \text{ mg cm}^{-2}$  is assumed.

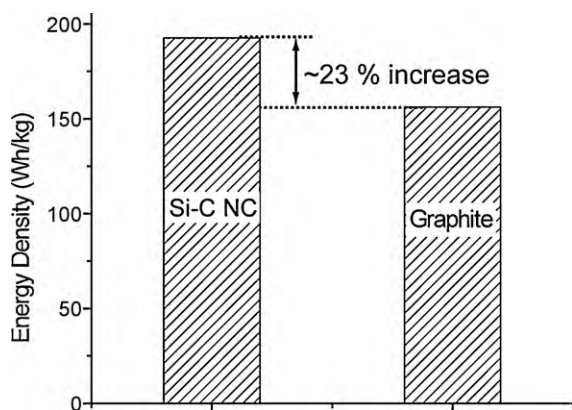


**Fig. 4.** Specific energy densities of CNF-SiNW nanocomposite and commercial graphite-based cells when areal capacities are fixed to the typical commercial value of  $4 \text{ mAh cm}^{-2}$ . The detailed calculation is shown in Table S1 of Supplementary Materials.

components are assumed to be fixed for a full cell with an areal capacity of  $4 \text{ mAh cm}^{-2}$ , a specific energy density improvement of  $\sim 23\%$  is achieved (Fig. 4). Detailed information on the mass of each component and energy density calculation are shown in Table 2 and Supplementary Materials. Furthermore, the volumetric capacities of our nanocomposites appear superior to those of commercial counterparts. The thickness of our CNF-SiNW nanocomposite is  $\sim 35 \mu\text{m}$ . As shown in Fig. 3C, the cell with a  $3.6 \text{ mg cm}^{-2}$  mass loading shows the areal capacity of  $\sim 5 \text{ mAh cm}^{-2}$ . Thus, the volumetric capacity is  $\sim 1429 \text{ mAh cm}^{-3}$ . In practical 18,650 cells, the gravimetric capacity of graphite is  $\sim 350 \text{ mAh g}^{-1}$ . Considering the density of graphite is  $\sim 2.15 \text{ g cm}^{-3}$ , we can estimate the volumetric capacity and thickness of graphite layer to be  $\sim 750 \text{ mAh cm}^{-3}$  and  $\sim 50 \mu\text{m}$ , respectively. In actual cells, the thickness of graphite layer must be thicker than the simple calculation based on the material density and has been reported to be  $80\text{--}150 \mu\text{m}$  [2]. Therefore, the volumetric capacities of commercial anodes are  $250\text{--}470 \text{ mAh cm}^{-3}$ . In typical cases, SiNWs are expected to have lower material densities at given volumes due to open space between NWs compared to commercial electrodes consisting of micron size particles. However, once SiNWs are grown in 3D porous platforms as in our study,

**Table 2**  
The mass of each component in commercial graphite and CNF-SiNW cells (full cell configuration) when the areal capacities are  $4 \text{ mAh cm}^{-2}$  (unit:  $\text{mg cm}^{-2}$ ).

	Commercial graphite	CNF-SiNW nanocomposite
Cu current collector	13.4	0
Anode active material	13.5	3
Al current collector	5.4	5.4
Cathode active material	28.5	28.5
Other components	40.55	40.55
All	101.35	77.45

the volumetric capacities can be improved beyond commercial values because the open space between NWs decreases significantly.

#### 4. Conclusions

In this study, we demonstrate the high capacity anode platform by developing a nanocomposite where both active material and current collectors consist of 1D nanomaterials. The absence of heavy current collectors leads to a remarkable weight reduction. Also, active material consisting of 1D SiNWs exhibit high capacities with a decent cycle life due to the intrinsic advantage of silicon and facile strain relaxation via the 1D nanostructure. Moreover, the active material mass loading of the nanocomposites increases significantly compared to flat substrates, and thus the areal capacities of these cells become comparable to those of commercial cells ( $>4 \text{ mAh cm}^{-2}$ ). For this type of nanocomposite to be a viable option for large scale batteries, the sheet resistances must be reduced further. As we demonstrated previously, this issue could be overcome by including 1D metal nanowires in the ink as well as developing a novel cell design with global current collectors [3]. It is also noteworthy that 3D carbon nanofoam structures that are already commercially available and used for various applications [19] can be used as platforms for this type of nanocomposite device but scaled up to larger sizes.

#### Acknowledgements

This work was supported from the King Abdullah University of Science and Technology (KAUST) Investigator Award (No. KUS-11-001-12). J. M. acknowledges funding support from the National Science Foundation Graduate Research Fellowship and the National Defense Science and Engineering Graduate Fellowship.

#### Appendix A. Supplementary data

Supplementary data associated with this article can be found, in the online version, at doi:10.1016/j.jpowsour.2010.06.108.

#### References

- [1] J.M. Tarascon, M. Armand, Nature 414 (2001) 359–367.
- [2] B.A. Johnson, R.E. White, J. Power Sources 70 (1998) 48–54.
- [3] L.B. Hu, J.W. Choi, Y. Yang, S. Jeong, F. La Mantia, L.F. Cui, Y. Cui, Proc. Natl. Acad. Sci. 106 (2009) 21490–21494.
- [4] S. Bourderau, T. Brousse, D.M. Schleich, J. Power Sources 81 (1999) 233–236.
- [5] J.H. Ryu, J.W. Kim, Y.E. Sung, S.M. Oh, Electrochem. Solid-State Lett. 7 (2004) A306–A309.
- [6] J. Graetz, C.C. Ahn, R. Yazami, B. Fultz, Electrochem. Solid-State Lett. 6 (2003) A194–A197.
- [7] B.C. Kim, H. Uono, T. Satou, T. Fuse, T. Ishihara, M. Ue, M. Senna, J. Electrochem. Soc. 152 (2005) A523–A526.
- [8] I.S. Kim, P.N. Kumta, J. Power Sources 136 (2004) 145–149.
- [9] M.H. Park, M.G. Kim, J. Joo, K. Kim, J. Kim, S. Ahn, Y. Cui, J. Cho, Nano Lett. 9 (2009) 3844–3847.
- [10] L.F. Cui, Y. Yang, C.M. Hsu, Y. Cui, Nano Lett. 9 (2009) 3370–3374.

- [11] C.K. Chan, H.L. Peng, G. Liu, K. McIlwrath, X.F. Zhang, R.A. Huggins, Y. Cui, *Nat. Nanotechnol.* 3 (2008) 31–35.
- [12] J.W. Choi, J. McDonough, S. Jeong, J.S. Yoo, C.K. Chan, Y. Cui, *Nano Lett.* 10 (2010) 1409–1413.
- [13] V.I. Chani, Q. Yang, D.S. Wilkinson, G.C. Weatherly, *J. Power Sources* 142 (2005) 370–381.
- [14] M.N. Obrovac, L.J. Krause, *J. Electrochem. Soc.* 154 (2007) A103–A108.
- [15] P. Poizot, S. Laruelle, S. Grugeon, L. Dupont, J.M. Tarascon, *Nature* 407 (2000) 496–499.
- [16] M. Wachtler, J.O. Besenhard, M. Winter, *J. Power Sources* 94 (2001) 189–193.
- [17] K.D. Kepler, J.T. Vaughey, M.M. Thackeray, *J. Power Sources* 81 (1999) 383–387.
- [18] S. Hossain, Y.K. Kim, Y. Saleh, R. Loutfy, *J. Power Sources* 114 (2003) 264–276.
- [19] A.E. Fischer, K.A. Pettigrew, D.R. Rolison, R.M. Stroud, J.W. Long, *Nano Lett.* 7 (2007) 281–286.